MNRAS **451,** 611–621 (2015) doi:10.1093/mnras/stv953

An emerging population of BL Lacs with extreme properties: towards a class of EBL and cosmic magnetic field probes?

G. Bonnoli,[1⋆] F. Tavecchio,[1] G. Ghisellini[1] and T. Sbarrato[1,2]

[1] *INAF – Osservatorio Astronomico di Brera, via E. Bianchi 46, I-23807 Merate, Italy*

[2] *Dipartimento di Fisica 'G. Occhialini', Università di Milano Bicocca, Piazza della Scienza 3, I-20126 Milano, Italy*

Accepted 2015 April 28. Received 2015 April 28; in original form 2014 December 19

ABSTRACT

High-energy observations of extreme BL Lac objects, such as 1ES 0229+200 or 1ES 0347−121, recently focused interest both for blazar and jet physics and for the implication on the extragalactic background light and intergalactic magnetic field estimate. However, the number of these extreme highly peaked BL Lac objects (EHBL) is still rather small. Aiming at increase their number, we selected a group of EHBL candidates starting from the BL Lac sample of Plotkin et al. (2011), considering those undetected (or only barely detected) by the Large Area Telescope onboard *Fermi* and characterized by a high X-ray versus radio flux ratio. We assembled the multiwavelength spectral energy distribution of the resulting nine sources, profiting of publicly available archival observations performed by *Swift*, *GALEX*, and *Fermi* satellites, confirming their nature. Through a simple one-zone synchrotron self-Compton model we estimate the expected very high energy flux, finding that in the majority of cases it is within the reach of present generation of Cherenkov arrays or of the forthcoming Cherenkov Telescope Array.

Key words: radiation mechanisms: non-thermal – galaxies: active – galaxies: jets – gamma-rays: galaxies.

1 INTRODUCTION

Intense emission of γ-rays is a distinctive feature of blazars, active galactic nuclei (AGN) dominated by the boosted non-thermal continuum from a relativistic jet pointed towards the observer. The 2LAC catalogue (Ackermann et al. 2011), listing the AGN detected with high significance by the Large Area Telescope (LAT) onboard *Fermi* during its first two years of operations, contains 886 sources, of which 862 are blazars (395 sources classified as BL Lacs, 310 Flat Spectrum Radio Quasars, and 157 sources of 'unknown type'). Blazars also dominate the extragalactic sky at very high energy (VHE, $E > 100$ GeV) with BL Lac being the dominant population (58 over a total of 67 extragalactic sources discovered until 2014 November according to TeVCat[1], Wakely & Horan 2008). Within BL Lacs, the large majority (51 out of 58) of the VHE emitters belongs to the High-peaked BL Lac (HBL) subclass.

The spectral energy distribution (SED) of blazars displays two characteristics broad humps, whose peak frequency appears to anti-correlate with the emitted power (Fossati et al. 1998, but see Giommi et al. 2005). While the low-energy (from radio up to optical) emission is clearly associated with synchrotron radiation, the nature of the mechanisms responsible for the high-energy continuum is still debated. The majority of the studies adopts the so-called leptonic scenario, in which the high-energy radiation is interpreted as the product of the inverse Compton (IC) scattering of the relativistic electrons and soft photons (either produced internally, i.e. the synchrotron photon themselves, or externally to the emitting region). Hadronic models (Böttcher et al. 2013) instead assume that the γ-ray emission is either the byproduct of reactions initiated by ultrarelativistic hadrons and mediated by mesons (e.g. Atoyan & Dermer 2003; Mücke et al. 2003) or direct synchrotron emission from protons (e.g. Aharonian 2000).

For the great majority of known BL Lac objects the high-energy component peaks in the 1–100 GeV band. However, there is a small group of sources detected at TeV energies by Cherenkov arrays for which the maximum is located above 1 TeV (e.g. Tavecchio et al. 2011). The extreme hardness of the spectrum makes these sources very faint and thus often undetected in the LAT band. These features can be exploited to effectively constrain the intergalactic magnetic field (IGMF; e.g. Dolag et al. 2009; Neronov & Vovk 2010; Tavecchio et al. 2010, 2011; Dermer et al. 2011; Vovk et al. 2012; Oikonomou, Murase & Kotera 2014). Other properties shared by these sources are the extremely large ratio between the X-ray and the radio flux and the hardness of the X-ray continuum ($\Gamma \sim 2$), locating the synchrotron peak in the medium-hard X-ray band. These characteristics lead to collect them under the term

⋆ E-mail: giacomo.bonnoli@brera.inaf.it

[1] http://tevcat.uchicago.edu

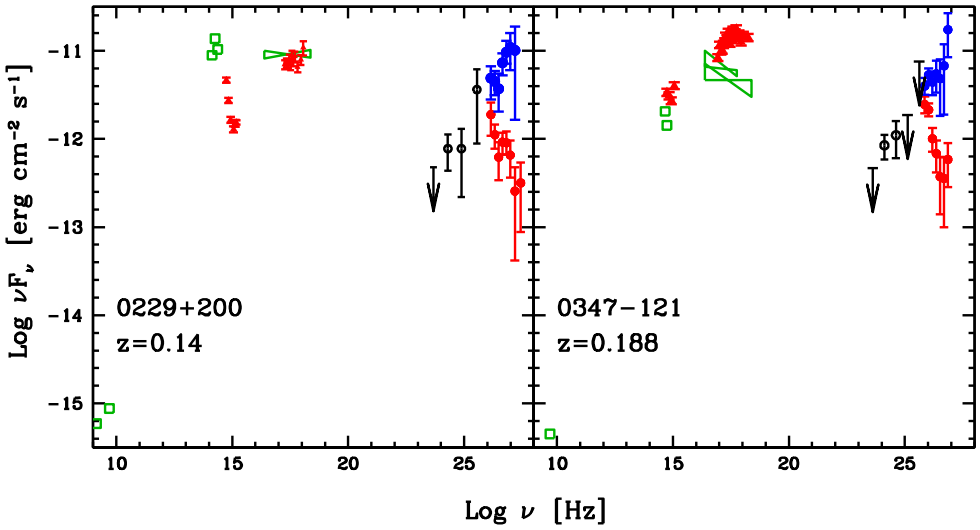

Figure 1. SED of 1ES 0229+200 (left) and 1ES 0347−121 (right), two of the most representative EHBL detected at TeV energies (see Tavecchio et al. 2011 for references). Blue symbols show the TeV spectrum corrected for the absorption by EBL using the model of Domínguez et al. (2011). The black points for 1ES 0229+200 report the *Fermi*/LAT spectrum obtained by Vovk et al. (2012), while those for 1ES 0347−121 come from Tanaka et al. (2014).

'extreme' HBL (EHBL; Costamante et al. 2001). In the IR-optical regime the emission is dominated by the host galaxy and the non-thermal jet continuum starts to be important only in the UV band. The modelling of their SED within the synchrotron self-Compton (SSC) framework reveals rather unusually low magnetic fields ($B < 0.01$ G) and large electron energies (Tavecchio et al. 2010, 2011). The emitted hard TeV spectrum (once corrected for interaction with the extragalactic background light, EBL) can be reproduced assuming that the electron energy distribution is truncated below a minimum Lorentz factor around $\gamma_{\rm min} \sim 10^5$ (Katarzyński et al. 2005; Tavecchio et al. 2009, 2011; Kaufmann et al. 2011). This interpretation also accounts for the peculiar UV/X-ray spectrum. Alternatively, the SED could be the result of a Maxwellian electron distribution (Lefa, Rieger & Aharonian 2011), internal absorption (Aharonian, Khangulyan & Costamante 2008; Zacharopoulou et al. 2011) or IC scattering between electrons and photons of the cosmic microwave background in the large-scale (∼kpc) jet (Böttcher, Dermer & Finke 2008). Alternatively lepto-hadronic models can be also invoked, either through proton–synchrotron emission, or through secondary cascades inside the emission region initiated by ultrarelativistic hadrons (see e.g. Cerruti et al. 2015). A last suggestive possibility is that high-energy photons are produced by ultra-high energy protons along the line of sight injected by the blazars into the intergalactic space (Essey et al. 2011; Murase et al. 2012a; Zheng & Kang 2013; Tavecchio 2014).

From the brief description given above is clear that EHBL are rather interesting objects, both for the study of jets phenomenology or even Ultra High Energy Cosmic Ray astrophysics and for the use of probes of EBL and IGMF. However, their use is somewhat hampered by the small number of EHBL detected at TeV energies. This is the main fact driving this work, in which we intend to characterize a group of EHBL detectable at TeV energies by present instruments or by the upcoming Cherenkov Telescope Array (CTA; Acharya et al. 2013). Sparse groups of EHBL have been identified in previous work (e.g. Giommi et al. 2005; Nieppola, Tornikoski & Valtaoja 2006). Here, we intend to follow a focused and well-defined selection procedure, based on the compilation of the SDSS/FIRST BL Lac of Plotkin et al. (2011), and the criterion of an extreme radio-to-X-ray flux ratio (Section 2). We show their SED using recent *Swift* data (Section 3). We also profit from archival *Galaxy Evolution Explorer* (*GALEX*) satellite data and we analyse the whole *Fermi*/LAT photon archive in order to constrain their behaviour in γ-rays by computing at least upper limits if no detection is possible, which comes out to be the most common result, in agreement with our expectations. Based on a simple SSC homogeneous model we reproduce the resulting SED (Section 4), giving also an estimate of their flux and detectability for Imaging Atmospheric Cherenkov Telescopes (IACT) of the present and forthcoming generation.

Throughout the paper, we assume the following cosmological parameters: $H_0 = 70$ km s^{-1} Mpc^{-1}, $\Omega_{\rm M} = 0.3$, $\Omega_\Lambda = 0.7$. We use the notation $Q = Q_X\, 10^X$ in cgs units.

2 SELECTION OF TEV CANDIDATES EHBL

The SED of two representative EHBL detected in the TeV band, 1ES 0229+200 and 1ES 0347−121, are reported in Fig. 1.[2] To select EHBL candidates we are guided by two evident peculiarities of these SED, namely the large X-ray/radio flux ratio and a non-thermal optical continuum lower than the thermal contribution from the galaxy. These two features suggest to select EHBL among the BL Lacs with high X-ray/radio flux ratio whose optical spectrum is dominated by the galaxy.

We emphasize that this criterion should not be confused with the one adopted in Costamante & Ghisellini (2002) who aimed to maximize the TeV flux (with a selection based on the evidence of large X-ray and radio fluxes), while here we tend, in a wide sense, to minimize the TeV spectral index. The criterion is rather model independent, as it arises by similarity with the archetypal EHBL 1ES 0229+200 and 1ES 0347−121 mentioned above. In the scope of a pure one-zone SSC model (e.g. Tavecchio, Maraschi & Ghisellini 1998), this can be interpreted as the outcome of an electron distribution characterized by high minimum ($\gamma_{\rm min}$) and break ($\gamma_{\rm b}$) Lorentz factors; this translates into large values of the peak frequencies for

[2] Note that due to a bug in the calculation of the effective area, the X-ray spectrum reported in Tavecchio et al. (2009) was too high. In Fig. 1 the correct spectrum is shown.

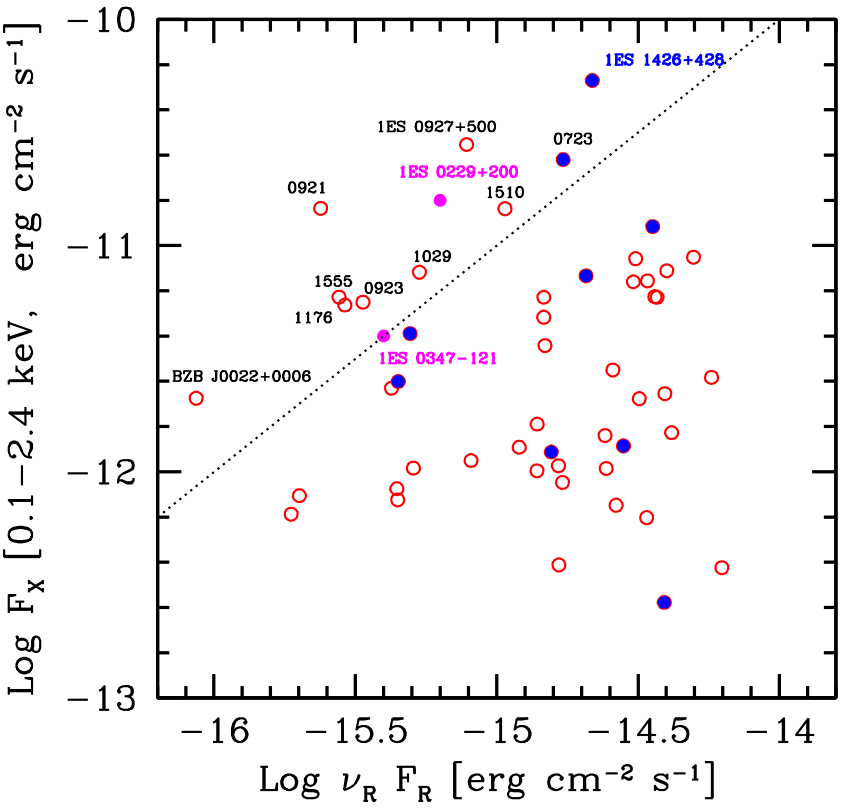

Figure 2. F_X versus F_R diagnostic plot for the sample of BL Lacs described in the text. Red open circles represent the full sample; the blue filled circles are the LAT detected ones. The 12 sources above the black dotted diagonal line have a high ($F_X/F_R > 10^4$) ratio of X-ray versus radio flux. The magenta filled circles are the two archetypal TeV detected, but GeV faint extreme BL Lacs, 1ES 0229+200 (Vovk et al. 2012) and 1ES 0347−121 (Tanaka et al. 2014).

the synchrotron (ν_s) and IC (ν_{IC}) components of the radiation spectrum, and dim (due to scarcity of seed photons) but hard TeV spectra. Costamante & Ghisellini (2002) instead requested both high-energy electrons and seed photons to be abundant in the emission region, in order to maximize the bolometric VHE luminosity. This interpretation suggests that the regions of the F_X/F_r parameter space plotted in Fig. 2 selected by the two criteria should actually host BL Lac populations of different flavour, with the TeV-brightest clustered towards the upper-right corner while the TeV-hardest clustered at the upper-left corner. While the Costamante & Ghisellini (2002) selection has been robustly proved by the detection at TeV energies of most of their candidate sources, the one we adopt here will need extensive observation of the selected sources in order to be proven or rejected.

Guided by this criterion, we started our selection from the list of 71 BL Lac presented by Plotkin et al. (2011) resulting from the correlation of SDSS and FIRST surveys and by optical spectrum dominated by the host galaxy emission; to enforce this, we limit the study within $z = 0.4$. To apply our criteria we further select those with measured X-ray flux (by *ROSAT*), from Plotkin et al. (2010), obtaining a total of 50 BL Lacs. Note that the cut in redshift, originally dictated by the requirement of the galaxy dominance in the optical band, also ensures that the relatively small suppression of the EBL for γ-rays up to a few TeV does not prevent detection by current Cherenkov arrays.

The X-ray flux in the 0.1–2.4 keV band and the radio flux at 1.4 GHz (expressed as $F_R \equiv \nu F_\nu$ for homogeneity with the integrated X-ray flux), of the sources resulting from the selection have been taken from Plotkin et al. (2010) and are reported in Fig. 2. There, the blue points show the sources already detected by LAT (2FGL catalogue). For comparison, the magenta points report the fluxes of 1ES 0229+200 and 1ES 0347−121 (although not belonging to our selected sources). The oblique dashed line corresponds to a fixed ratio $F_X/F_R = 10^4$. This particular, rounded but somewhat arbitrary value is suggested by the position of the two known EHBL in the plane. The sources above the line are expected to be good EHBL candidates, without any claim for completeness, as we are not aiming at it at this level. For instance, just outside of the region and next to 1ES 0347−121 lies RBS 1049, which would easily fit in the same scheme. In this region, there are two sources already detected by LAT, RBS 0723 and 1ES 1426+428. The latter is already a well established TeV source (Horan et al. 2002). Although its SED is coherent with our picture, it can be considered a transition object towards the 'bright X-ray'–'bright radio' corner of the plot, populated by the bright blazars of Costamante & Ghisellini (2002) therefore will be omitted in the following discussion. It is worth noticing that 1ES1426+428 is not a standalone case, as another hard source not belonging to our sample but to the one of Giommi et al. (2005) that is built along a similar line has been discovered at VHE by HESS (SHBL J001355.9−185406 at $z = 0.095$; H.E.S.S. Collaboration et al. 2013). More recently RBS 0723 has been discovered at VHE too, by MAGIC (Mirzoyan 2014). Other extreme BL Lacs such as those contemplated in Cerruti et al. (2015) also show X-ray to radio flux ratios high enough to fit in the scheme.

In Table 1, we report the names of the selected EHBL together with their coordinates and redshifts. Note that, as an indirect result of the selection, requiring a bright X-ray emission, most of them belong to the Rosat Bright Survey (RBS; Voges et al. 1999).

Table 1. List of the extreme blazar candidates selected from the sample of Plotkin et al. (2011). For each source the equatorial (J2000) and galactic coordinates are reported (in degrees), the redshift and the A_B extinction coefficient from Schlegel, Finkbeiner & Davis (1998). As a consequence of the selection within SDSS, all the sources lie at high-galactic latitudes.

Source Name	R.A.(J2000)	δ(J2000)	l	b	Redshift	A_B
BZB J0022+0006	5.5040	0.1161	107.18	−61.85	0.306	0.108
RBS 0723	131.8039	11.5640	215.46	30.89	0.198	0.093
1ES 0927+500	142.6566	49.8404	168.19	45.71	0.187	0.073
RBS 0921	164.0275	2.8704	249.28	53.28	0.236	0.178
RBS 0923	164.3462	23.0552	215.96	63.91	0.378	0.088
RBS 1029	176.3963	−3.6671	273.11	55.34	0.168	0.130
RBS 1176	193.2540	38.4405	121.36	78.68	0.371	0.083
RBS 1510	233.2969	18.9081	29.21	52.05	0.307	0.210
RBS 1555	241.3293	54.3500	84.35	45.60	0.212	0.041

3 MULTIWAVELENGTH DATA

For the sources fulfilling our criterion on the F_X/F_R ratio we built multiwavelength SED exploiting publicly available data. We used archival optical–UV data from *Swift*/UVOT and soft X-ray data from *Swift*/XRT for the vast majority of the sources, while for RBS 0921 and RBS 1176 we requested dedicated *Swift* observations. We also profited from the *GALEX* archive[3]. Other data have been also added using the ASI Science Data Center (ASDC) archive[4]. All the considered sources have been observed at least one time with *Swift*, ensuring a good description of the crucial UV–X-ray band. No particular attempt was made to seek for strictly simultaneous observations, that would need a dedicated observational campaign, being these sources generally reputed of secondary importance and therefore left aside from any monitoring campaign of some time density.

We also analysed *Fermi*/LAT data. Almost all the sources are undetected and we could only calculate upper limits.

In the following, we describe the analysis performed on the *Swift*/XRT *Swift*/UVOT and *Fermi*/LAT data.

3.1 *Swift*/XRT data

Swift/XRT (Burrows et al. 2005) observations were available for all the sources in our subsample, except for RBS 0923 and RBS 1176, which were targets of dedicated observations: RBS 0923 was observed in 2012 July, while RBS 1176 was observed in 2011 November, then in 2012 May and June. For most of the other sources only one observation was available, except for RBS 1029 which was observed in 2007 November and December, 1ES0927+500, observed in 2010 September and 2011 March, and RBS 1510 in 2011 June, September, October and in 2012 January.

Swift/XRT data were analysed by using the HEASOFT v. 6.13 software package with the CALDB updated on 2013 January 21 and processed with XRTPIPELINE v. 0.12.6 with standard parameters. Spectra have been grouped to have at least 20 counts per bin, in order to use the χ^2 test and analysed with XSPEC v. 12.8.0 in the 0.3–10 keV energy band.

For all sources (with perhaps the exception of RBS 1176, see below) an absorbed power-law model provides a good description of the spectrum. In the majority of cases the absorption column can be fixed to the Galactic value (Kalberla et al. 2005).

In Table 2, we report the results of the fitting procedure. In the two cases of 1ES 0927+500 and RBS 1029 we separately consider two spectra. The best-fitting parameters are perfectly consistent. All the other multiple data sets could be merged as no hint of variability was found.

More complex is the case of RBS 1176. A fit of the summed spectrum with a power-law model returns an absorption column N_H largely in excess to the Galactic value (Table 2). Alternatively, a good fit ($\chi^2/d.o.f. = 12.46/13$) can be obtained assuming a broken power-law model and the Galactic value of N_H, with slopes $\Gamma_1 = 1.1 \pm 0.3$, $\Gamma_2 = 2.3 \pm 0.3$ and break energy $E_b = 1.3 \pm 0.3$ keV. The spectra of the single pointings are much less constraining. A single power-law model (with photon index $\Gamma \sim 1.7$) with Galactic absorption is barely compatible with the data but a curved spectrum is clearly suggested by the shape of the residuals.

3.2 *Swift*/UVOT data

Swift/UVOT (Roming et al. 2005) is a 30 cm diffraction-limited optical–UV telescope, equipped with six different filters, sensitive in the 1700–6500 Å wavelength range, in a 17 arcmin × 17 arcmin FoV. We retrieved from the High Energy Astrophysics Science Archive Research Center (HEASARC) data base the UVOT images in which our target sources were observed. The maximum angular distance from the optical axis does not exceed 4 arcmin for any source.

For all the sources and the available different observations the analysis was performed with the `uvotimsum` and `uvotsource` tasks with a source region of 5 arcsec, while the background was extracted from a source-free circular region with radius equal to 50 arcsec. The extracted magnitudes were corrected for Galactic extinction using the values of Schlegel et al. (1998), reported in the last column of Table 1 and applying the formulae by Pei 1992 for the UV filters, and eventually were converted into fluxes following Poole et al. 2008.

Table 3 reports the observed Vega magnitudes in the *Swift*/UVOT v, b, u, $m1$, $m2$, and $w2$ filters, together with statistical uncertainties. Systematic uncertainties are never greater than 0.03 mag and therefore dominated by statistical ones in the vast majority of cases.

3.3 *Fermi*/LAT data

Publicly available *Fermi*/LAT data were retrieved from the Fermi Science Support Center (FSSC) and analysed by means of the LAT Science Tools v. 9.27.1, together with the Instrument

[3] http://galex.stsci.edu/galexview/
[4] http://tools.asdc.asi.it/

Table 2. Results of the *Swift*/XRT data analysis for all the archival observations of our sample available until the end of 2012 August. The table reports: source name, exposure time (expressed in *s*), best-fitting value of spectral index of power-law model, column density (in units of 10^{20} cm^{-2}), χ^2 and degrees of freedom of the best fit, flux in the 0.3–10 keV band (in units of 10^{-12} erg cm^{-2} s^{-1}). [1] For this source $N_{H,\,gal} = 1.72 \times 10^{20}$ cm^{-2}.

Source name	Obs. ID	Exp. time (s)	Γ	N_H (10^{20} cm^{-2})	χ^2/d.o.f.	$F_{0.3-10\,keV}$ (10^{-12} erg cm^{-2} s^{-1})
BZB J0022+0006	38113001	4700	2.40 ± 0.25	2.76 (Gal.)	7.19/8	1.7 ± 0.3
RBS 0723	37396001	2000	1.78 ± 0.12	3.17 (Gal.)	20.8/18	2.6 ± 0.3
1ES 0927+500 1	39154001	2870	2.0 ± 0.1	1.38 (Gal.)	40.13/37	14 ± 1
2+3	39154002-3	2260	2.2 ± 0.1	1.38 (Gal.)	29.4/33	16 ± 1
RBS 0921	37547001	4700	1.89 ± 0.08	3.82 (Gal.)	44.8/46	8.4 ± 0.4
RBS 0923	48001001-4	6400	2.2 ± 0.1	1.12 (Gal.)	25.8/26	3.6 ± 0.3
RBS 1029 1	36813001	2900	2.2 ± 0.2	2.22 (Gal.)	8.1/6	2.7 ± 0.3
2	36813002	2900	2.0 ± 0.1	2.22 (Gal.)	9.35/10	3.2 ± 0.2
RBS 1176	48000001-3	5250	2.3 ± 0.3	13.3 ± 6.5[1]	14.1/13	2.7 ± 0.3
RBS 1510	91101001-5	3700	2.2 ± 0.1	3.83 (Gal.)	35.0/33	8.3 ± 0.6
RBS 1555	38303001	7100	2.0 ± 0.1	0.886 (Gal.)	23.4/29	1.7 ± 0.1

Table 3. *Swift*/UVOT observed magnitudes for all the archival observations of our sample available until the end of 2012 August. Statistical uncertainties only are reported: systematic error is always within 0.03 mag and almost generally dominated by statistical ones.

Source name	Obs. ID	*v*	*b*	*u*	*w*1	*m*2	*w*2
BZB J0022+0006	38113001	19.23 ± 0.17	–	19.17 ± 0.10	–	–	19.38 ± 0.09
RBS 0723	37396001	17.60 ± 0.11	18.49 ± 0.10	17.65 ± 0.08	17.39 ± 0.07	17.49 ± 0.08	17.43 ± 0.05
1ES 0927+500	39154001-3	–	–	17.32 ± 0.03	–	–	17.97 ± 0.04
RBS 0921	37547001	18.78 ± 0.33	19.02 ± 0.17	18.63 ± 0.16	18.79 ± 0.12	18.95 ± 0.12	18.92 ± 0.07
RBS 0923	48001001-4	18.97 ± 0.19	19.67 ± 0.15	18.82 ± 0.09	18.59 ± 0.09	18.68 ± 0.1	18.6 ± 0.08
RBS 1029	36813001-2	–	–	18.47 ± 0.06	–	–	18.73 ± 0.05
RBS 1176	48000001-3	19.49 ± 0.21	20.05 ± 0.15	19.53 ± 0.13	19.35 ± 0.13	19.10 ± 0.13	19.52 ± 0.14
RBS 1510	91101001-5	–	–	–	17.54 ± 0.04	17.51 ± 0.05	17.65 ± 0.04
RBS 1555	38303001	19.37 ± 0.11	–	19.69 ± 0.13	–	–	19.99 ± 0.11

Response Function Pass 7 and the corresponding isotropic and Galactic diffuse background models. Source (class 2) photons in the 0.1–100 GeV energy range, collected until 2012 August 21 and coming from direction within 10° from the nominal position of the source were selected and filtered through standard FSSC quality cuts. Standard analysis steps were then performed, eventually adopting the *test statistic* from Mattox et al. (1996) to assess the significance of excess signal in correspondence with our targets. Besides the target (modelled as a simple power law) and backgrounds, all the 2FGL point sources in the field were included in the model.

Most of the sources were undetected on the whole 0.1–100 GeV energy band. For RBS 1510 (TS = 23.0) and 1ES0927+500 (TS = 24.5), we had marginal detections while we could confirm RBS 0723, already present in both the 1FGL and 2FGL catalogues. Then we computed fluxes in the 1–10 GeV and 10–100 GeV bands, relaxing the limit for a detection to TS>9 for the sources that were detected in the full band; however, none of the others reached this threshold in either energy bin. In absence of a measured flux we computed 2σ upper limits, following Rolke, López & Conrad (2005). Results are collected in Table 4 and plotted in Figs 3–5. In the last two columns we also report the number of photons with energy $E > 10$ GeV detected within a 0.°4 radius (roughly corresponding to 68 per cent containment for $E > 10$ GeV) from the nominal position of the source, and the energy of the most energetic one E_{max}. A rigorous study of the significance of these photons, taking into account the different point spread function of LAT for front and back converted photons, aiming to check and exclude contamination from nearby hard sources (though unlikely) and eventually to assess the probability of enclosing background photons within the same aperture, was beyond the scope of this work.

3.4 *GALEX* data

The *GALEX* (Martin et al. 2005) was a NASA Small Explorer, in flight since 2003 April 28, and operational until mid-2013.

It performed an all-sky survey in the far-UV (FUV, $\lambda_{eff} \sim 154$ nm) and near-UV (NUV, $\lambda_{eff} \sim 232$ nm) band. We retrieved from the Multimission archive at the Space Telescope Science Institute (MAST)[5] archival fluxes observed for the sources of our sample (see Table 5). No data is found for RBS 1176, likely due to a gap in the sky coverage of the survey.

4 SPECTRAL ENERGY DISTRIBUTIONS

The SED of the sources are reported in Figs 3–5. In all cases we use the same colour code: green symbols are used for archival data from ASDC, red points for *Swift*/XRT, UVOT, and LAT data and black triangles for *GALEX* data (taken from the data base). Note that in almost all cases the *GALEX* and UVOT data in the UV filters perfectly agree, in spite of the uncorrelated observing epochs. The only exception is RBS 1510 for which *GALEX* provides fainter fluxes than UVOT. In this case variability is likely an explanation for this difference.

[5] Multimission Archive at the Space Telescope Science Institute, http://galex.stsci.edu

Table 4. Results of our analysis of the *Fermi*/LAT data collected until 2012 August 21 for the sources of our EHBL sample. For each target in the first three columns the integral flux above 0.1 GeV, the slope of the simple power-law model and the TS are reported. Then the value of the flux or the 2σ U.L. in the 1–10 GeV and 10–100 GeV energy bins are reported. In the last two columns, the number of photons with $E > 10$ GeV observed within 0.°4 from the nominal position of the source, and the energy $E_{\rm max}$ the most energetic one.

Source name	$F_{0.1-100\,\rm GeV}$ (10^{-10} ph cm^{-2} s^{-1})	Γ	TS	$F_{1-10\,\rm GeV}$ (10^{-10} ph cm^{-2} s^{-1})	$F_{10-100\,\rm GeV}$ (10^{-10} ph cm^{-2} s^{-1})	Hard photons ($N_{E>10\,\rm GeV}$)	$E_{\rm max}$ (GeV)
BZB J0022+0006	–	–	1.88	<1.7	<0.4	1	31.5
RBS 0723	11.3 ± 2.6	1.46 ± 0.08	79	3.9 ± 1.0	0.69 ± 0.25	10	77.6
1ES 0927+500	4.2 ± 3.4	1.38 ± 0.3	24.5	<1.4	0.62 ± 0.26	9	159.1
RBS 0921	–	–	4	<2.4	<0.44	2	23.4
RBS 0923	–	–	3	<1.5	<0.36	1	53.7
RBS 1029	–	–	0.002	<2.0	<0.29	0	–
RBS 1176	–	–	−0.04	<2.3	<0.31	1	13.7
RBS 1510	5.8 ± 3.6	1.48 ± 0.21	23.0	2.0 ± 0.8	0.36 ± 0.20	5	42.9
RBS 1555	–	–	0.44	<2.0	<0.39	2	10.9

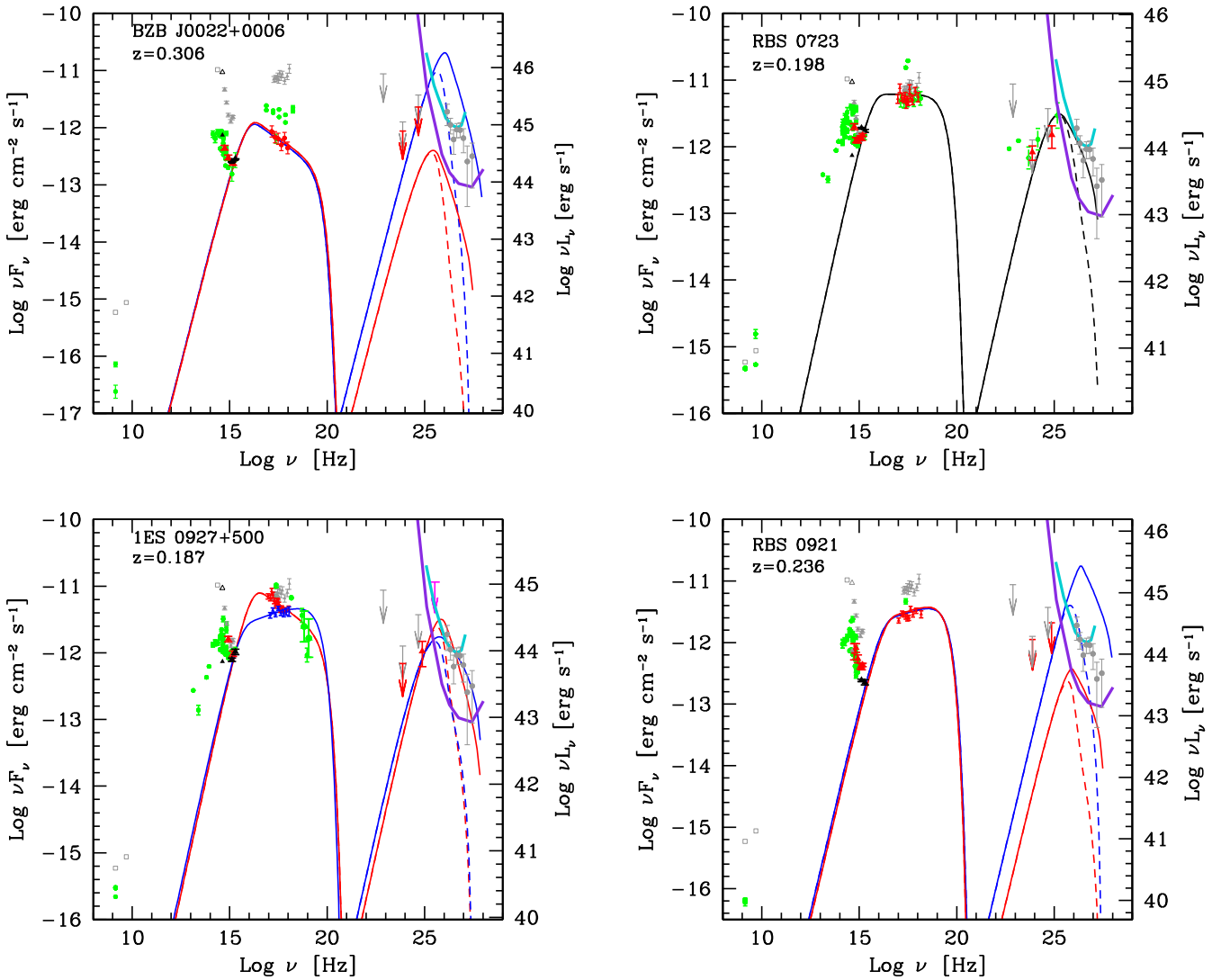

Figure 3. SED of the selected extreme BL Lac objects. Green symbols reports historical data from ASI/ASDC archive. Red symbols show *Swift*/UVOT, XRT, and *Fermi*/LAT data discussed in the text. Black symbols display *GALEX* data. Background grey symbols show the SED of 1ES 0229+200 for comparison. For sources not detected by LAT, we report two different models of the SED, corresponding to low ($B = 0.01$ G, blue lines) and high ($B = 0.1$ G, red lines) magnetic field. For sources with a LAT detection we only report one model, in black (parameters are reported in Table 6). For 1ES 0927+500 we report two models, corresponding to the two X-ray slopes (see Table 2). Dashed lines show the model after absorption with the EBL, calculated according to Domínguez et al. (2011). Light blue and violet curves report the differential sensitivities (5σ, 50 h of exposure, 5 bins per energy decade) of MAGIC and CTA, respectively.

Table 5. Archival *GALEX* fluxes in the FUV and NUV bands for our sample of EHBL. No data is found for RBS 1176, likely due to a gap in the sky coverage of the survey.

Source name	FUV flux (μJy)	NUV flux (μJy)
BZB J0022+0006	17.0 ± 0.2	23.40 ± 0.25
RBS 0723	104.3 ± 4.9	177.2 ± 4.3
1ES 0927+500	59.3 ± 5.6	68.8 ± 4.1
RBS 0921	15.1 ± 1.5	25.4 ± 1.1
RBS 0923	12.6 ± 3.7	22.8 ± 3.5
RBS 1029	17.5 ± 4.3	32.9 ± 4.9
RBS 1176	–	–
RBS 1510	24.9 ± 6.2	48.1 ± 5.3
RBS 1555	9.62 ± 0.51	11.3 ± 0.2

For comparison, we report in background (grey) the data corresponding to 1ES 0229+200 (for simplicity only the observed TeV spectrum is shown). It is clear that the structure of the synchrotron part of the SED of all the sources closely resembles that of 1ES 0229+200. In all cases the steep optical continuum is dominated by the host galaxy emission. A feature shared by all the sources is the large ratio between the flux in the UV band and soft X-ray band. As remarked in Tavecchio et al. (2009, see also Kaufmann et al. 2011), in the framework of the one-zone leptonic model, this features can be reproduced if the energy distribution of the emitting electrons is truncated below a relatively large value, $\gamma_{\rm min} = 10^{4-5}$. As for 1ES 0229+200, this also causes a very hard SSC component, consistent with the extremely low flux in the LAT band.

As discussed in Section 3.1, for RBS 1176 the observed deficit of soft X-ray photons in the XRT spectrum can be interpreted either as due to intrinsic or intervening absorption or as the evidence for an intrinsic curvature of the spectrum. In the latter case, the extremely hard soft X-ray continuum (photon index close to 1) would be readily interpreted in the SSC scheme as the synchrotron low-energy tail of the electrons with Lorentz factor $\gamma_{\rm min}$. In this case, RBS 1176 would thus be a source characterized by a peculiarly large $\gamma_{\rm min}$, for which the break in the synchrotron continuum – which in the other sources occurs between the UV and the X-ray bands – is located around 1 keV. Therefore, RBS 1176 could be the first example of *ultraextreme HBL*.

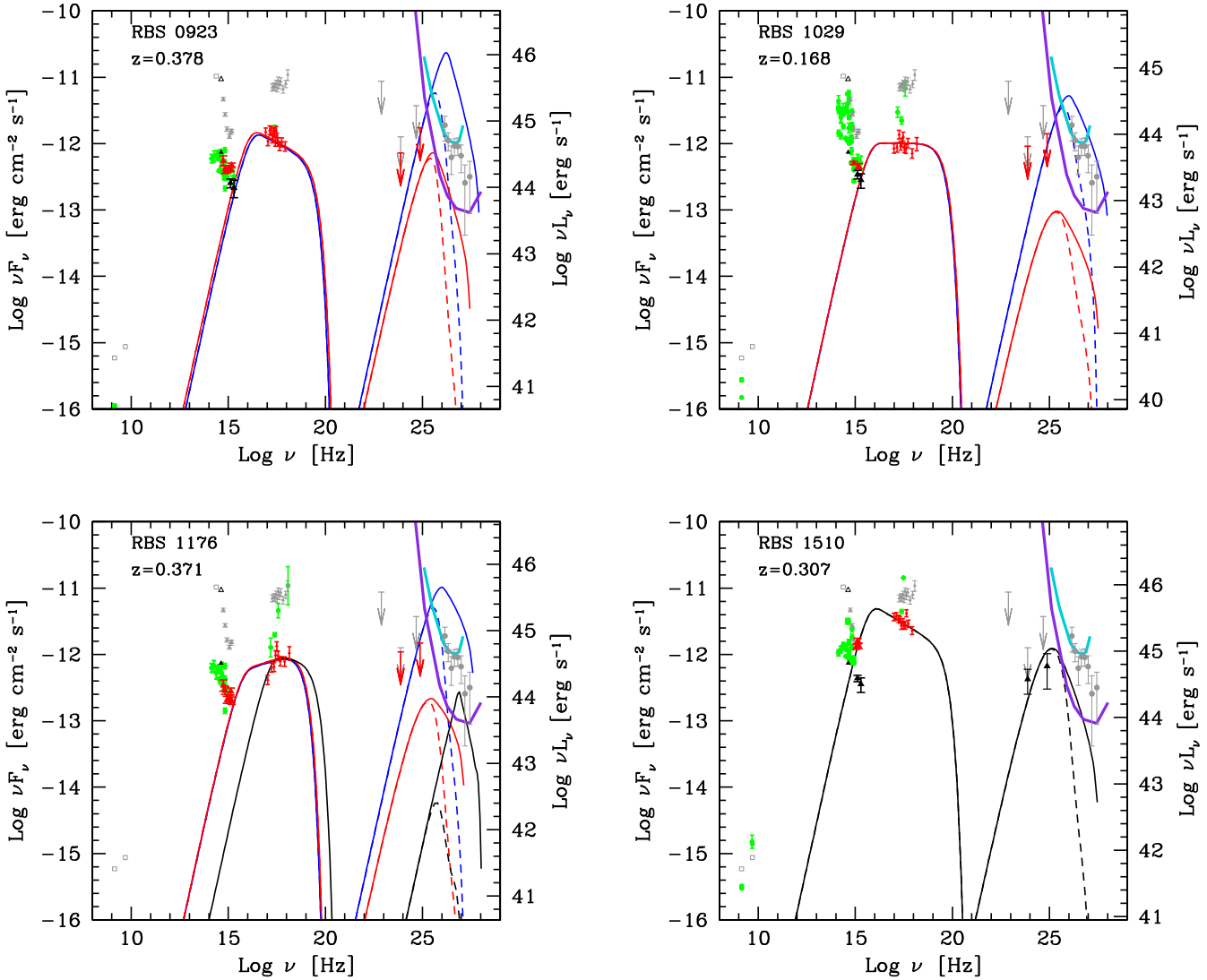

Figure 4. As in Fig. 3. In the case of RBS 1176, the black line refers to the model assuming the highest value of $\gamma_{\rm min}$ compatible with the X-ray spectrum ($\gamma_{\rm min} = 4 \times 10^5$, see Table 6).

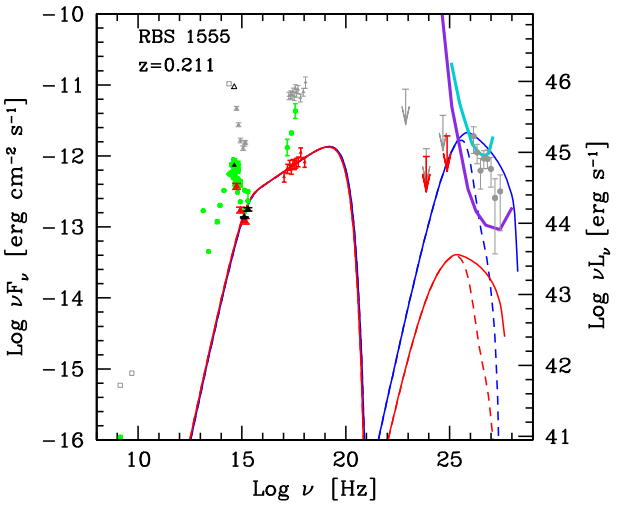

Figure 5. As Fig. 3.

Our selection criterion is rather efficient in selecting EHBL blazars, as shown by the similarity of the synchrotron SEDs of the selected sources, even if the paucity of the γ-ray data does not allow (yet) a detailed comparison of the high-energy SEDs. We remark that the selection procedure does not explicitly require that the synchrotron peak is in the X-ray band (which is the defining feature of EHBL). Nevertheless, almost all the selected BL Lacs show hard X-ray spectra, often showing photon indices below 2, locating the synchrotron peak energy above 10 keV; it is worth noticing that with indices around 2 the position of the synchrotron peak can shift a lot (from $\sim 10^{16}$ to $\sim 10^{19}$ Hz), even if the synchrotron luminosity is almost constant. As shown below, the exact location of the synchrotron peak does not affect much the predicted TeV flux, since this depends mostly on the low-energy edge of the electron distribution (see the case of 1ES 0927+500 below).

The high-energy component is unconstrained in almost all the sources, with the exception of RBS 0723, RBS 1510, and 1ES 0927+500, detected by LAT at the highest energies. Based on the striking similarity of the synchrotron bump, it is reasonable to assume that the high-energy component is also similar to that of 1ES 0229+200, characterized by an extremely hard spectrum in the LAT ($\Gamma = 1.36 \pm 0.25$ according to Vovk et al. 2012, but see Cerruti et al. 2015 where a softer slope is found) and TeV bands. This assumption is supported by the detection of 1ES 0927+500 and RBS 1510 only at high energy and by the hard photon index of RBS 0723 reported in the 2FGL, $\Gamma = 1.48 \pm 0.16$. In the next paragraph we then estimate the expected TeV flux assuming as SED template and physical parameters those of 1ES 0229+200.

4.1 SED Modelling and predicted TeV fluxes

We use the one-zone leptonic model of Tavecchio et al. (1998), fully described in Maraschi & Tavecchio (2003). The emitting region is assumed to be spherical with radius R, filled by a tangled magnetic field of intensity B. To reduce the number of free parameters we assume that the relativistic electrons follow a simple power-law distribution $N(\gamma) = K\gamma^{-n}$ with $\gamma_{\rm min} < \gamma < \gamma_{\rm max}$. As for the case of 1ES 0229+200 (Tavecchio et al. 2009; Kaufmann et al. 2011) this distribution suitably describes the observed SED. The relativistic beaming of the synchrotron and SSC radiation is described by the relativistic Doppler factor δ. These parameters fully specify the model, that can be uniquely fixed once the quantities specifying the two bumps (peak frequencies and

Table 6. Physical parameters describing the jet emission in our sample within the framework of the SSC model from Tavecchio et al. (1998), with the simplifying assumption that the energy spectrum of the emitting electrons follows a simple (instead of broken) power-law distribution. A common Doppler factor $\delta = 20$ is assumed for all the sources. For each target source the intensity of the magnetic field within the emission region B, the electron spatial density K, the minimum and maximum electron energy $\gamma_{\rm min}$ and $\gamma_{\rm max}$, the slope of the power-law distribution n are reported. [1]: $R = 6.5 \times 10^{15}$ cm, $\delta = 30$; [2] the first two lines refer to the model assuming a power-law X-ray spectrum. The third line is for a broken power-law X-ray spectrum (black line in Fig. 4); [3]:$R = 1.4 \times 10^{16}$ cm.

Source name	B (G)	K	$\gamma_{\rm min}$	$\gamma_{\rm max}$	n
BZB J0022+0006	0.1	1.7×10^{11}	3×10^4	2×10^6	3.5
	0.01	2.75×10^{13}	9×10^4	6×10^6	3.5
RBS 0723	0.15	6×10^8	2.1×10^4	1.5×10^6	3.0
1ES 0927+500[1] 1	0.05	1.7×10^{10}	4.1×10^4	3×10^6	3.3
2+3	0.035	1.3×10^7	2.7×10^4	3×10^6	2.7
RBS 0921	0.1	8×10^7	4.7×10^4	1.8×10^6	2.8
	0.01	6×10^9	1.3×10^5	6×10^6	2.8
RBS 0923	0.1	1.4×10^8	2.2×10^4	2×10^6	3.3
	0.01	5.1×10^{12}	1.2×10^5	5.2×10^6	3.3
RBS 1029	0.1	1.4×10^8	2.2×10^4	2×10^6	3.0
	0.01	1.4×10^{10}	7×10^4	6×10^6	3.0
RBS 1176[2]	0.1	6×10^7	2.3×10^4	10^6	2.8
	0.01	4.6×10^9	7.3×10^4	3×10^6	2.8
	0.01	3×10^{11}	4×10^5	3×10^6	3.1
RBS 1510[3]	0.12	6.2×10^9	2×10^4	2×10^6	3.35
RBS 1555	0.1	1.2×10^6	1.3×10^4	3×10^6	2.6
	0.01	7.5×10^7	4.3×10^4	10^7	2.6

luminosities, spectral slopes) and the variability time-scale are known (Tavecchio et al. 1998).

In the present case, since in the majority of cases we do not have any direct measurement of the high-energy hump, it is not possible to uniquely derive the physical parameters of the emitting sources. Moreover the minimum variability time-scale $t_{\rm var}$ for these sources is not known, thus allowing additional degeneracy in the $K-R$ plane. On the other hand, relying on the physical parameters inferred for known EHBL (e.g. Tavecchio et al. 2011), it is possible to derive the SSC component and thus an estimate of the expected TeV flux. According to the results of the models in Tavecchio et al. (2010, 2011), we then fix the radius $R = 6 \times 10^{15}$ cm and the Doppler factor $\delta = 20$. Then we consider two values of the magnetic field bracketing the expected range of the magnetic field intensity, $B = 0.01$–0.1 G and for each value we derive the remaining parameters (n, K, $\gamma_{\rm min}$ and $\gamma_{\rm max}$) reproducing the synchrotron component (described by the X-ray spectrum and the UV data) and the upper limits in the GeV band. The only parameter loosely constrained in this procedure is $\gamma_{\rm max}$, which, however, has only a minor impact on the derived SSC component due to Klein–Nishina suppression. For 1ES 0927+500, RBS 0723 and RBS 1510, the LAT data allow us to constrain also the level of the SSC component and to determine all the parameters. Therefore in this case, we present only one model. For RBS 1176, as discussed above, we consider both possibilities for the X-ray spectrum. For the case assuming additional absorption we report two models, as for the other sources. For the case in which the X-ray continuum as an intrinsic curvature we show one model (black lines), assuming $B = 0.01$ G. We do not consider the case of a larger magnetic field for which the SSC luminosity (already low) would be much smaller.

As discussed in Katarzyński et al. (2005) and Tavecchio et al. (2009), the peculiar SED of EHBL can be reproduced in the framework of the standard one-zone leptonic model assuming that the emitting relativistic electrons follow an energy distribution truncated below a relatively large energy or, equivalently, Lorentz factor $\gamma_{\rm min}$. In this case, below the typical synchrotron frequency of electrons with Lorentz factor $\gamma_{\rm min}$, $\nu_{\rm min} \simeq 2.8 \times 10^6 B \gamma_{\rm min}^2 \delta$, the resulting spectrum is described by the characteristics hard power law $F(\nu) \propto \nu^{1/3}$. The same hard spectrum describes the SSC emission up to the peak energy $h\nu_{\rm C} \simeq \gamma_{\rm min} m_{\rm e} c^2\, \delta$. Since the UV and X-ray data constrain $\nu_{\rm min}$ around 10^{16} Hz, the typical minimum Lorentz factor is $\gamma_{\rm min} \simeq 2 \times 10^5 \nu_{\rm min,16}^{1/2} B_{-2}^{-1/2} \delta_1^{-1/2}$, implying a SSC peak at $\nu_{\rm C} \simeq 1\, \nu_{\rm min,16}^{1/2} B_{-2}^{-1/2} \delta_1^{1/2}$ TeV. Note that in this scheme the sources with very large separation between the X-ray and the UV fluxes, implying a large value of $\nu_{\rm min}$, are expected to have the maximum of the SSC component at VHE and are thus the most promising sources for TeV detection. Larger values of δ have been sometimes required in the past to model the SED of HBL, (e.g. Aleksić et al. 2012), and would boost even more the detectability of our sources.

4.2 Results

The resulting theoretical SED are shown by the red ($B = 0.1$ G) and blue ($B = 0.01$ G) lines in Figs 3–5. Solid lines report the intrinsic emission, dashed lines show the observed emission, corrected for absorption through interaction with the EBL using the model of Domínguez et al. (2011). We note here that the radio emission cannot be explained by our model, providing fluxes well below the measured level. This is a general feature of single-region models, which are especially intended to model the emission at higher frequencies emitted by compact components. The low frequency radio emission is instead likely produced in extended regions in the jet.

The cases with low B are characterized by a larger SSC flux and vice versa. This is simply due to the well-known fact that the ratio between the SSC and synchrotron luminosities is proportional to the radiation and magnetic energy densities, i.e. $L_{\rm SSC}/L_{\rm syn} = U_{\rm rad}/U_B$. For a fixed $L_{\rm syn}$ also $U_{\rm rad}$ is constant, thus $L_{\rm SSC} \propto B^{-2}$.

Figs 3–5 also display the sensitivity curves for MAGIC (light blue; Sitarek et al. 2013) and CTA (violet; Actis et al. 2011) corresponding to 50 h of observation and 5σ significance. It is noteworthy that these sensitivity curves assume a 0.2 dex energy binning; therefore, dimmer flux densities are still within reach if a more coarse binning is adopted. In the low magnetic field case, the majority of the sources could be already detected by the present generation of IACT and all the sources could be easily detected by CTA (Acharya et al. 2013). In the high B-field case, instead, the selected EHBL could be hard to detect even by CTA. However, we remark that the prediction of the SSC flux for the case of high magnetic field, $B = 0.1$ G, should be considered rather pessimistic, since the magnetic field intensity derived for most of the known EHBL tends to lie close to the low value $B = 10^{-2} G$ (e.g. Tavecchio et al. 2011).

For RBS 1176, the case of an intrinsic X-ray break results in a large peak frequency (which we recall is directly related to $\gamma_{\rm min}$, that in this case is larger than for the other sources) and a quite low SSC luminosity (related to the small energy density of the target optical-IR photons). Therefore, if the observed lack of soft photons is really connected to the intrinsic spectrum RBS 1176 (making this source the first ultraextreme HBL), we do not expect that it can easily detected by the CTA.

5 DISCUSSION

EHBLs are particular interesting for several reasons, ranging from the study of jet physics to the estimate of EBL and IGMF. In this work, we have assembled a well-defined group of EHBL and we have characterized their SED using historical, *Swift*, *Fermi*/LAT and (when available) *GALEX* data. All the SEDs closely resemble in shape that of the 'prototypical' EHBL 1ES 0229+200, demonstrating the efficiency of our selection in identify these kind of sources. We applied a simple one-zone synchrotron SSC model, trying to predict the flux at very high energies, showing that most of the sources could be detectable by the upcoming CTA. Given the shape of the SED, the most effective instruments of the CTA to detect EHBL would be the array of Medium Sized Telescopes (MST), dominating the overall sensitivity from several hundreds of GeV up to few TeV. In case of detection a deep follow up with the Large Sized Telescopes sensitive down to few tens of GeV could measure the reprocessed flux and hence the IGMF under the hypothesis that the intrinsic emission does not interfere below 100 GeV. Possible different variability at high (dominated by the intrinsic) and low energies could help to separate the two components.

One of the most interesting features of EHBL is their exceptionally hard GeV–TeV spectrum, which in most of cases puts the maximum of the SSC component above few TeV. Here, following Katarzyński et al. (2005) and Tavecchio et al. (2009) we interpret the hard TeV spectrum, together with the extreme X-ray/UV flux ratio, as the result of the emission from an electron population with a large minimum Lorentz factor, $\gamma_{\rm min} \simeq 10^5$. As discussed in Tavecchio et al. (2009), the exceptionally large $\gamma_{\rm min}$ seem to challenge existing models for particle acceleration, which usually predicts

power-law non-thermal tails starting from much lower values (e.g. Sironi & Spitkovsky 2011).

Another intriguing point is the apparent stability of the TeV spectrum over several years (Aharonian et al. 2007, but see also Aliu et al. 2014 for the case of 1ES 0229+200 where marginal evidence for mild TeV variability on a several months/annual time-scale is found), which neatly distinguishes EHBL from HBL that show rather variable TeV emission, down to time-scales of few minutes. As discussed in Tavecchio et al. (2009) for 1ES 0229+200 the radiative cooling time of electrons at $\gamma_{\rm min}$ is of the order of 2 yr, barely consistent with the observations. However, it is difficult to avoid other sources of losses, such as adiabatic losses. One interesting possibility to understand such a stable spectrum (e.g. Essey et al. 2011; Taylor, Vovk & Neronov 2011; Murase et al. 2012a) is that the GeV–TeV continuum is not the primary emission from the source, but instead is reprocessed radiation from cascading processes spread into the intergalactic space. Electromagnetic cascades could be the result of the absorption of primary multi-TeV γ-rays or, instead, could be produced by Bethe–Heitler pair creation or photomeson reactions involving ultrahigh energy protons accelerated in the source and beamed towards the Earth. As shown in Tavecchio (2014), the physical parameters of the jets are consistent with the requests of the hadronic cascade scenario, both in terms of maximum hadron energy and jet power. As discussed by Murase et al. (2012a) and Takami, Murase & Dermer (2013) an effective test to distinguish between intrinsic and reprocessed emission is the observation of photons at several TeV, only possible in the latter case, since the cascade emission, being produced at lower distance, is less affected by absorption than the intrinsic one; although exotic processes such as the photon–axion conversion (e.g. de Angelis, Galanti & Roncadelli 2011) could result in a lower effective absorption. Due to absorption and reprocessing of primary TeV photons a significant contribution to the GeV extragalactic gamma-ray background (EGB) could be related to EHBL (see e.g. Inoue & Ioka 2012; Murase, Beacom & Takami 2012b; Ajello et al. 2014). We plan to study this issue in a forthcoming paper.

Another topic worth of discussion is the position of these EHBLs within the general BL Lac population and the nature of their parent population. By construction, the sources we are discussing have very faint radio emission (radio luminosities around $L_r \sim 10^{40}$ erg s^{-1}) indicating very weak radio jets (e.g. Giroletti et al. 2004, for some sources). Considering that at least a fraction of the radio flux comes from the beamed jet synchrotron component, we argue that the intrinsic radio luminosity drops below the lower end of the FRI radiogalaxy power range, making EHBLs suitable candidates for the aligned counterparts of the weak radiogalaxies population studied by Baldi & Capetti (2009).

Finally, we wish to speculate on the existence of even more extreme EHBL. In fact it is tempting to suppose the existence of blazars which SED is shifted towards even higher energies, with the X-ray emission peak above 10 keV and high-energy component reaching several tens of TeV. Given the VHE of the synchrotron and IC peaks and low flux levels these sources could escape detection by *Swift* and *Fermi*. We speculate that possibly the CTA survey will allow us to detect or constrain this hypothetical subclass of the HBL population in the TeV band. Of course such sources would deeply suffer from EBL absorption around their IC emission peak, limiting their detectability at low redshifts and the detection of the left side of the IC bump below few TeV. Arguably, a relatively strong fraction of their radiated power would be reprocessed into the GeV band, setting limits to their spatial density. We will further investigate this issue in a future work.

A generalization of our criterion, for instance relaxing the condition of the known redshift, will allow us to validate this EHBL selection method on new and larger samples. This class of sources is especially important for improving our understanding about the far-IR EBL, IGMF, and EGB. Exploiting at the same time the capability of NuStar (Harrison et al. 2013), SKA (Carilli & Rawlings 2004), and CTA (Acharya et al. 2013) will be particularly revealing. Even before the completion of CTA, the planned ASTRI/CTA mini-array (Di Pierro et al. 2013; Vercellone et al. 2013) could be exploited in this direction. Actually, whereas the brightest flux from this sources is expected to be in the band up to 1 TeV, where MSTs will be the most sensitive instruments of CTA, still crucial physical information is engraved in the high-energy tail of the IC bump, in the band best observed with the Small Sized Telescopes.

For instance, these extreme sources could allow eventually to compare leptonic and hadronic emission scenarios in a multi-TeV territory where degeneracy of competing models is significantly reduced (see e.g. Murase et al. 2012a). Opportunity would arise for tests of non-standard physics such as violations of the Lorentz invariance (Fairbairn et al. 2014) or the speculated existence of axion-like particles (Meyer & Conrad 2014), once the number of these multi-TeV photon factories should become greater than now. Therefore, EHBL will be very interesting targets for challenging hot topics in fundamental physics, both with the ASTRI/CTA Mini–Array (improving the current H.E.S.S. sensitivity above 5 TeV) and with the full array of CTA small telescopes, which dominates the overall CTA sensitivity above the same threshold.

ACKNOWLEDGEMENTS

FT and GB acknowledge financial contribution from grant PRIN-INAF-2011. This work is based on the publicly available *Fermi*/LAT data obtained through the Science Support Center (SSC). This research has made use of data obtained from the HEASARC, provided by NASA's Goddard Space Flight Center. We acknowledge the use of public data from the Swift data archive. We also acknowledge use of *GALEX* data made publically available through the MAST. Part of this work is based on archival data, software or online services provided by the ASDC. We thank the referee Andreas Zech for comments that helped in improving the paper. We also acknowledge constructive comments from M. Cerutti, K. Murase, Y. Tanaka, and D. Sanchez.

REFERENCES

H. E. S. S. Collaboration et al., 2013, A&A, 554, A72
Acharya B. S. et al., 2013, Astropart. Phys., 43, 3
Ackermann M. et al., 2011, ApJ, 743, 171
Actis M. et al., 2011, Exp. Astron., 32, 193
Aharonian F. A., 2000, New Astron., 5, 377
Aharonian F. et al., 2007, A&A, 475, L9
Aharonian F. A., Khangulyan D., Costamante L., 2008, MNRAS, 387, 1206
Ajello M. et al., 2014, ApJ, 780, 73
Aleksić J. et al., 2012, A&A, 542, AA100
Aliu E. et al., 2014, ApJ, 782, 13
Atoyan A. M., Dermer C. D., 2003, ApJ, 586, 79
Baldi R. D., Capetti A., 2009, A&A, 508, 603
Böttcher M., Dermer C. D., Finke J. D., 2008, ApJ, 679, L9
Böttcher M., Reimer A., Sweeney K., Prakash A., 2013, ApJ, 768, 54
Burrows D. N. et al., 2005, Space Sci. Rev., 120, 165
Carilli C. L., Rawlings S., 2004, New Astron. Rev., 48, 979
Cerruti M., Zech A., Boisson C., Inoue S., 2015, MNRAS, 448, 910
Costamante L., Ghisellini G., 2002, A&A, 384, 56

Costamante L. et al., 2001, A&A, 371, 512
de Angelis A., Galanti G., Roncadelli M., 2011, Phys. Rev. D, 84, 105030
Dermer C. D., Cavadini M., Razzaque S., Finke J. D., Chiang J., Lott B., 2011, ApJ, 733, L21
Di Pierro F. et al., 2013, preprint (arXiv:1307.3992)
Dolag K., Kachelrieß M., Ostapchenko S., Tomàs R., 2009, ApJ, 703, 1078
Domínguez A. et al., 2011, MNRAS, 410, 2556
Essey W., Kalashev O., Kusenko A., Beacom J. F., 2011, ApJ, 731, 51
Fairbairn M., Nilsson A., Ellis J., Hinton J., White R., 2014, J. Cosmol. Astropart. Phys., 6, 005
Fossati G., Maraschi L., Celotti A., Comastri A., Ghisellini G., 1998, MNRAS, 299, 433
Giommi P., Piranomonte S., Perri M., Padovani P., 2005, A&A, 434, 385
Giroletti M., Giovannini G., Taylor G. B., Falomo R., 2004, ApJ, 613, 752
Harrison F. A. et al., 2013, ApJ, 770, 103
Horan D. et al., 2002, ApJ, 571, 753
Inoue Y., Ioka K., 2012, Phys. Rev. D, 86, 023003
Kalberla P. M. W., Burton W. B., Hartmann D., Arnal E. M., Bajaja E., Morras R., Pöppel W. G. L., 2005, A&A, 440, 775
Katarzyński K., Ghisellini G., Tavecchio F., Maraschi L., Fossati G., Mastichiadis A., 2005, A&A, 433, 479
Kaufmann S., Wagner S. J., Tibolla O., Hauser M., 2011, A&A, 534, A130
Lefa E., Rieger F. M., Aharonian F., 2011, ApJ, 740, 64
Maraschi L., Tavecchio F., 2003, ApJ, 593, 667
Martin D. C. et al., 2005, ApJ, 619, L1
Mattox J. R. et al., 1996, ApJ, 461, 396
Meyer M., Conrad J., 2014, J. Cosmol. Astropart. Phys., 12, 016
Mirzoyan R., 2014, Astron. Telegram, 5768, 1
Mücke A., Protheroe R. J., Engel R., Rachen J. P., Stanev T., 2003, Astropart. Phys., 18, 593
Murase K., Dermer C. D., Takami H., Migliori G., 2012a, ApJ, 749, 63
Murase K., Beacom J. F., Takami H., 2012b, J. Cosmol. Astropart. Phys., 8, 030
Neronov A., Vovk I., 2010, Science, 328, 73
Nieppola E., Tornikoski M., Valtaoja E., 2006, A&A, 445, 441
Oikonomou F., Murase K., Kotera K., 2014, A&A, 568, A110
Pei Y. C., 1992, ApJ, 395, 130
Plotkin R. M. et al., 2010, AJ, 139, 390
Plotkin R. M., Markoff S., Trager S. C., Anderson S. F., 2011, MNRAS, 413, 805
Poole T. S. et al., 2008, MNRAS, 383, 627
Rolke W. A., López A. M., Conrad J., 2005, Nucl. Instrum. Methods Phys. Res. A, 551, 493
Roming P. W. A. et al., 2005, Space Sci. Rev., 120, 95
Schlegel D. J., Finkbeiner D. P., Davis M., 1998, ApJ, 500, 525
Sironi L., Spitkovsky A., 2011, ApJ, 726, 75
Sitarek J. et al., 2013, preprint (arXiv:1308.0141)
Takami H., Murase K., Dermer C. D., 2013, ApJ, 771, L32
Tanaka Y. T. et al., 2014, ApJ, 787, 155
Tavecchio F., 2014, MNRAS, 438, 3255
Tavecchio F., Maraschi L., Ghisellini G., 1998, ApJ, 509, 608
Tavecchio F., Ghisellini G., Ghirlanda G., Costamante L., Franceschini A., 2009, MNRAS, 399, L59
Tavecchio F., Ghisellini G., Foschini L., Bonnoli G., Ghirlanda G., Coppi P., 2010, MNRAS, 406, L70
Tavecchio F., Ghisellini G., Bonnoli G., Foschini L., 2011, MNRAS, 414, 3566
Taylor A. M., Vovk I., Neronov A., 2011, A&A, 529, A144
Vercellone S. et al., 2013, preprint (arXiv:1307.5671)
Voges W. et al., 1999, A&A, 349, 389
Vovk I., Taylor A. M., Semikoz D., Neronov A., 2012, ApJ, 747, L14
Wakely S. P., Horan D., 2008, Int. Cosm. Ray Conf., 3, 1341
Zacharopoulou O., Khangulyan D., Aharonian F. A., Costamante L., 2011, ApJ, 738, 157
Zheng Y. G., Kang T., 2013, ApJ, 764, 113

This paper has been typeset from a TEX/LATEX file prepared by the author.